Supplementary Information

Robust Heat-insulating Organic-inorganic Hybrid Aerogel with a Green Preparation Strategy Inspired by Diatoms

Zibo Hua [a], Zhiqiang Wei [a], Ming Liu [a], Fanjun Guo [a], Tao You [a], Zidie Song [a], Ziqiao Wang [c], Yudong, Huang [a], Li Liu [ab]*, Mingqiang Wang [a]*

[a] *School of Chemistry and Chemical Engineering, Harbin Institute of Technology, Harbin 150001, P. R. China.*

[b] *State Key Laboratory of Advanced Inorganic Fibers and Composites, Harbin Institute of Technology, Harbin 150001, P. R. China*

[c] *Harbin FRP Institute, Harbin 150036, P.R. China.*

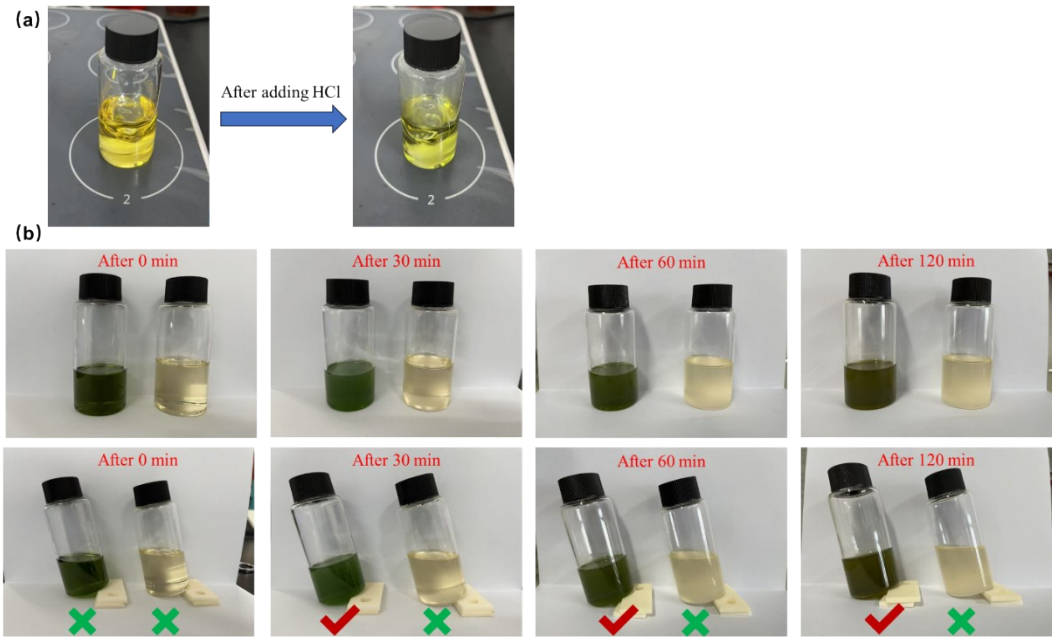

Fig. S1. Homogeneous and transparent hybridized sol

After adding acid catalyst, the colour of benzoxazine solution changes from yellow to light green, this process is very rapid, this is due to the high reactivity of benzoxazine. The gel system containing only benzoxazine monomers formed a gel earlier (30 min), while the gel system containing only MTMS did not have a gel at the same time.

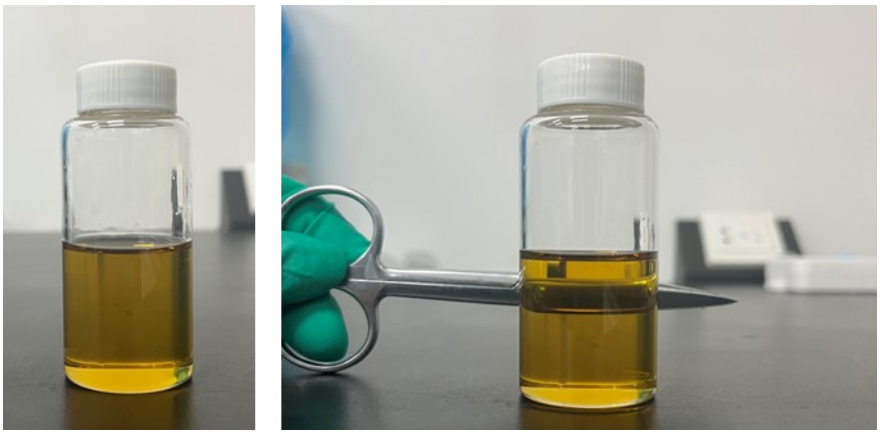

Fig. S2. Homogeneous and transparent hybridized sol

Hydrochloric acid first achieved ring-opening polymerization of Bz monomers, to which a certain degree of polymerization was added with an alkaline catalyst in order

to achieve rapid hydrolysis and condensation of siloxanes. Here the base catalyst we chose N-[3-(Trimethoxysilyl)propyl]ethylenediamine (KH-792), which contained both a basic amino group and could condense with siloxanes. A small amount of KH-792 did not affect the overall sol stability, as it can play the role of a base catalyst to accelerate the hydrolysis condensation reaction of local MTMS and participate in the polymerization.

To further confirm the important role of TA in the BSA sol-gel system, non-covalent bonding interactions were analyzed for benzoxazine monomer, hydrolyzed MTMS, and TA as shown in Fig. R1. Quantum chemical studies are performed using density functional theory (DFT) implemented in GAUSSIAN 16 package. Geometry optimization and frequency analysis are calculated at B3LYP hybrid functional with GD3BJ dispersion correlation at 6-31G(d) basis sets. Independent gradient model based on Hirshfeld partition (IGMH) are performed by Multiwfn 3.8 and VMD v 1.9.3 molecular visualization software, and the system binding energy was calculated as shown in Eq. 1.

$$E_b = E(AB) - E(A) - E(B) \quad (1)$$

Taking the binary systems A and B as an example, E_b in the above equation is the binding energy, E(AB) is the system energy of A and B after non-covalent interaction, and E(A) and E(B) are the system energies of each of A and B alone individually. For this work, A is BzM, B is hydrolyzed MTMS, C is TA.

Due to the excessive molecular weight of tannic acid, only one branched gallic acid structure was taken for simulation. After the addition of TA, TA interacted with

benzoxazine monomer as well as MTMS by non-covalent bonding, and the binding energy of the system was changed from -0.33 eV to -1.30 eV, which proved that the introduction of TA made the system more stable and was helpful in preventing the phase separation and gel inhomogeneity (**Fig. 1h**). In addition, the highly branched polyfunctional structure of the tannic acid molecules could further improve the capacity-enhancing effect and keep the sol-gel system stable under low viscosity conditions without the need to pre-polymerize the siloxane during the gelation process.

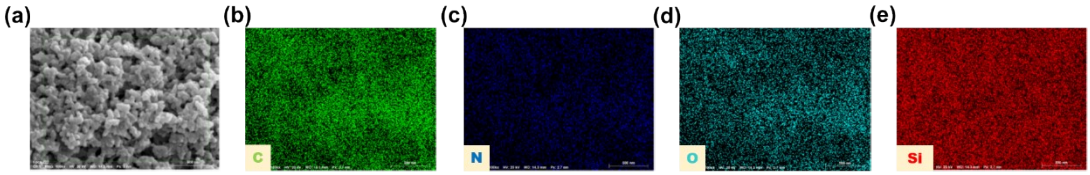

Fig. S3. EDS analysis images of BSA-1.5.

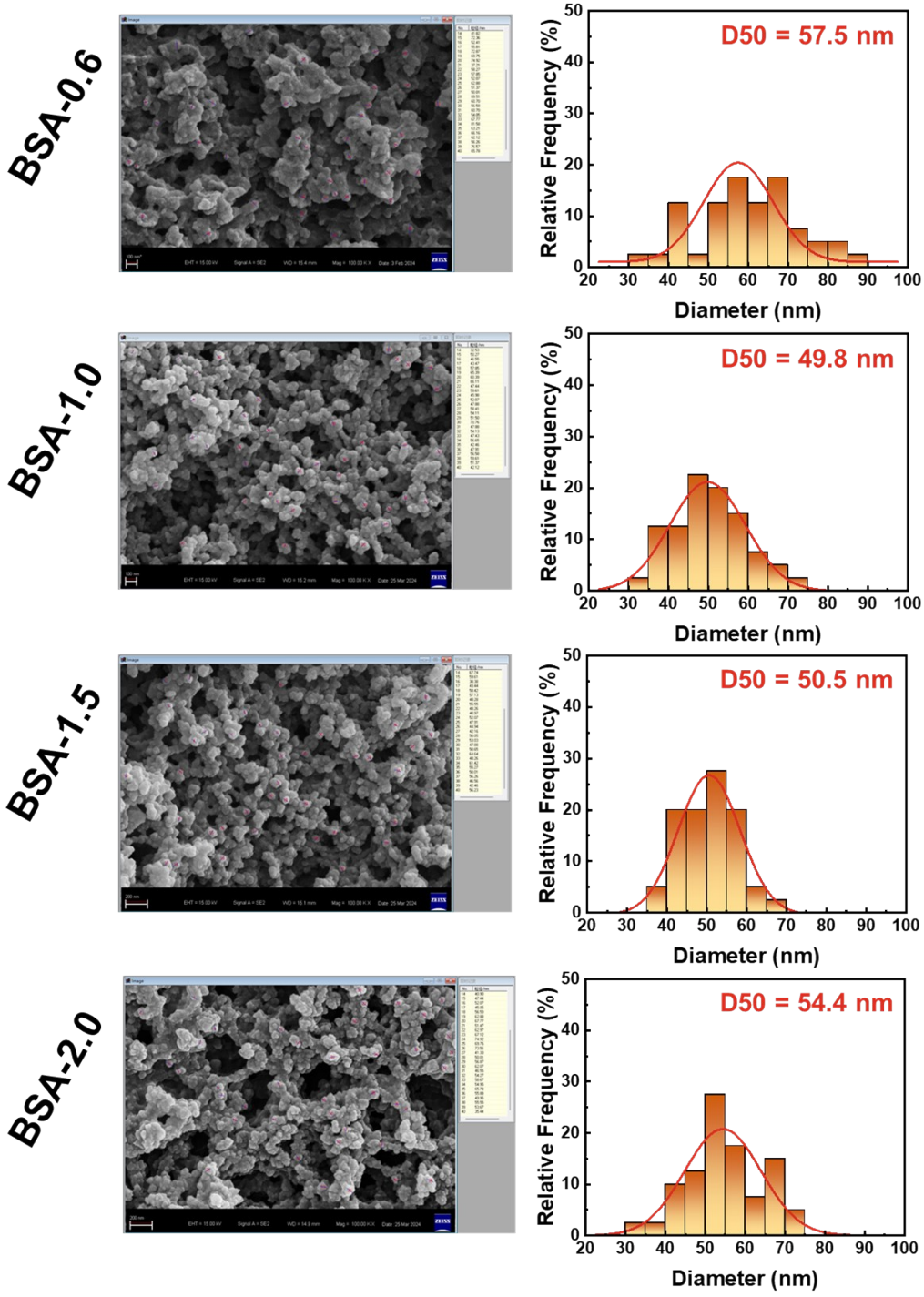

Fig. S4. Compositional particle size distribution of BSAs

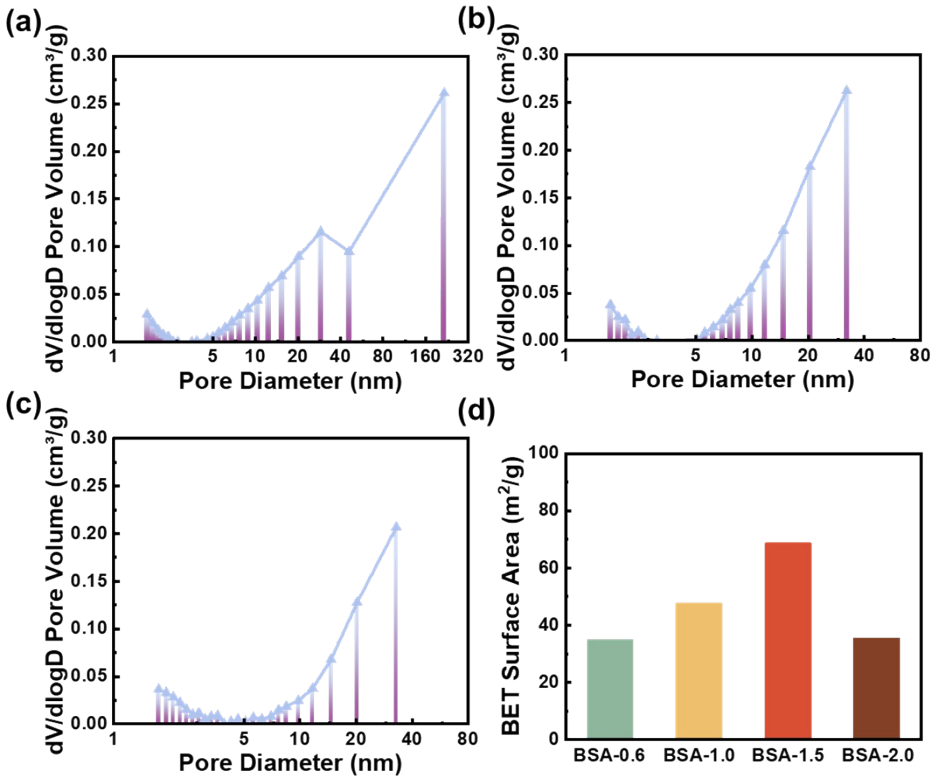

Fig. S5. BJH pore size distribution of BSA-0.6(a), BSA-1.0(b), BSA-2.0(c). (d) BET specific surface area of BSAs.

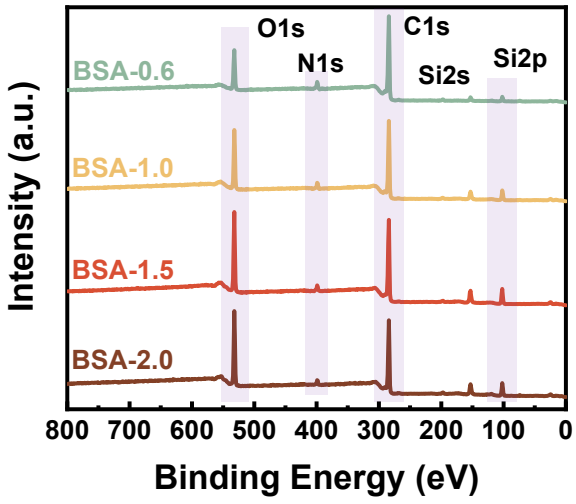

Fig. S6. XPS spectra of BSAs.

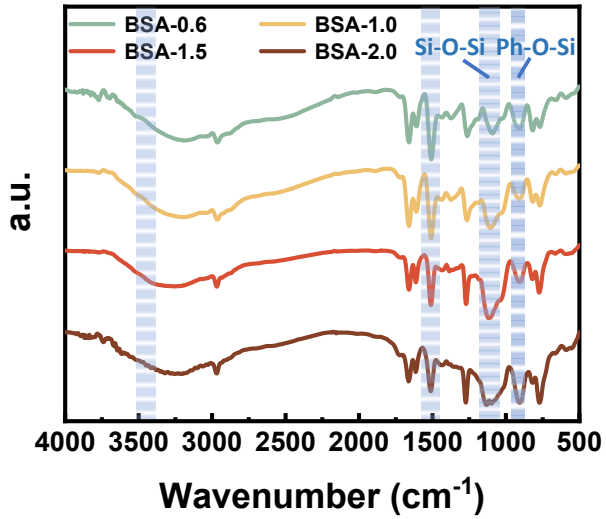

Fig. S7. Fourier Infrared Spectra of BSAs

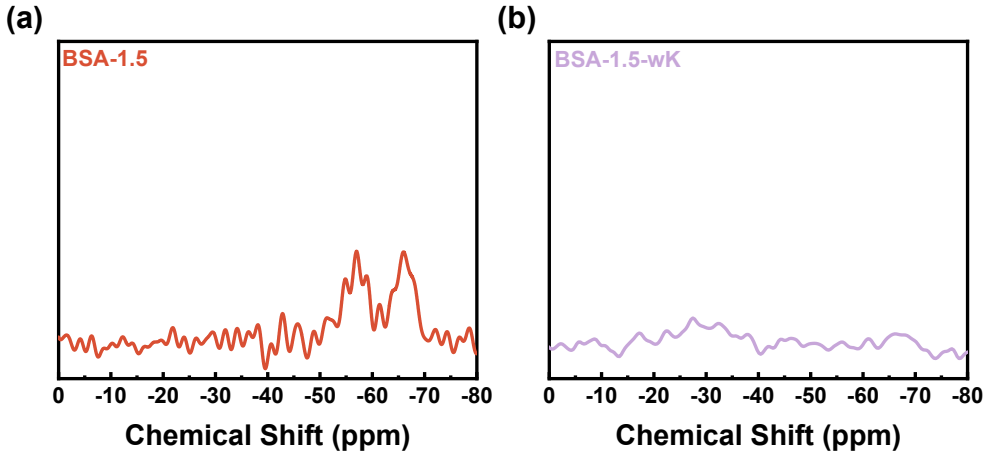

Fig. S8. ^{29}Si NMR spectra of BSA-1.5 (a) and BSA-1.5-wK (b)

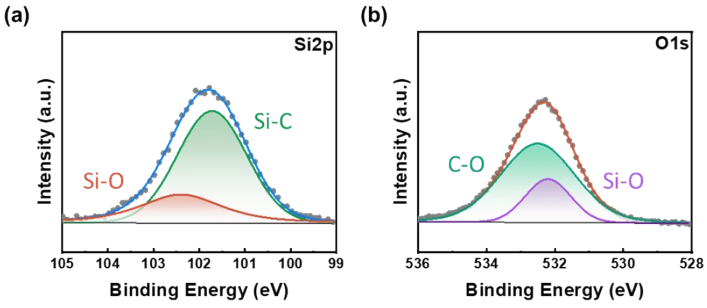

Fig. S9. XPS spectra of Si2p(a) and O1s(b) peaks of BSA-0.6.

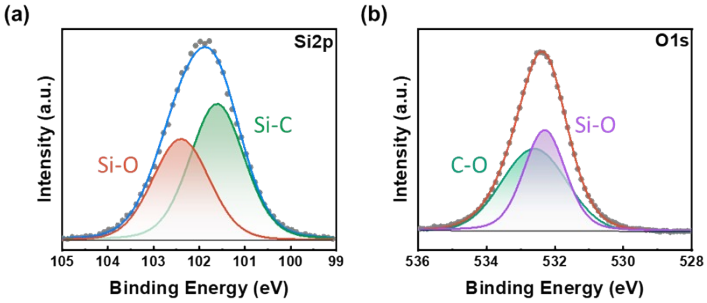

Fig. S10. XPS spectra of Si2p(a) and O1s(b) peaks of BSA-2.0.

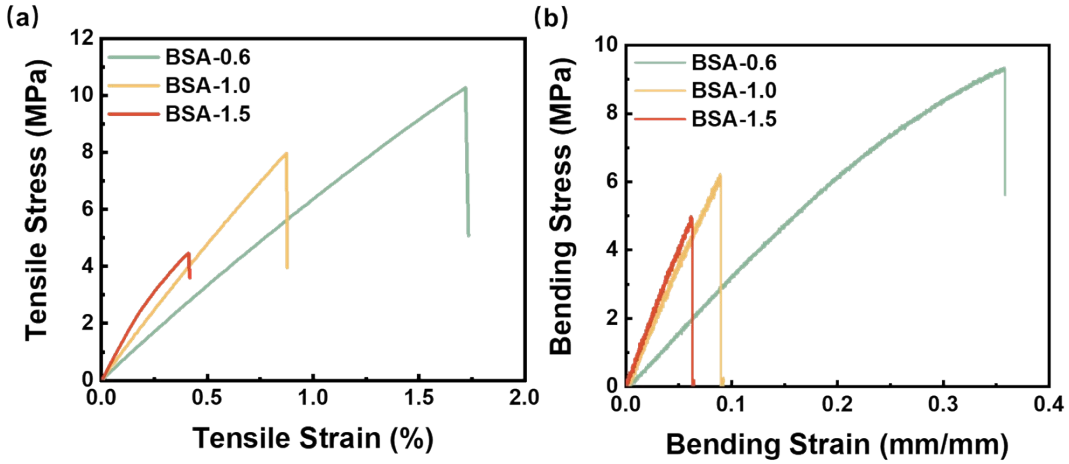

Fig. S11. (a) Tensile stress-strain curves of BSAs. (b) Bending stress-strain curves of BSAs

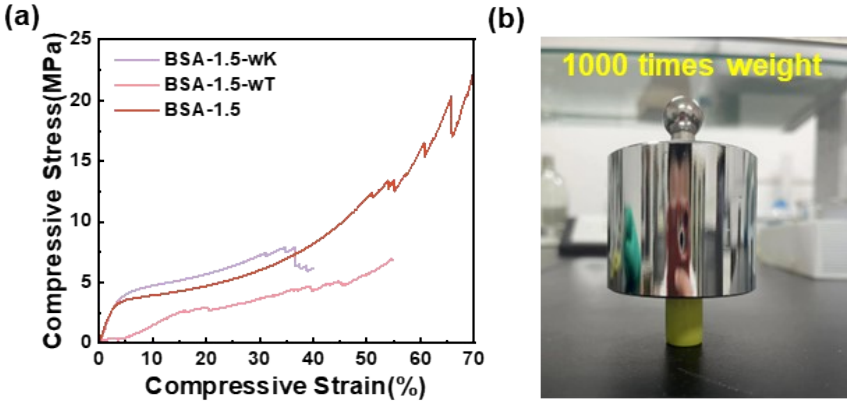

Fig. S12. (a) Compressive stress-strain curves of BSA-1.5-wK, BSA-1.5-wT, and BSA-1.5. (b) The 0.5 g BSA-1.5 carries a 500 g weight

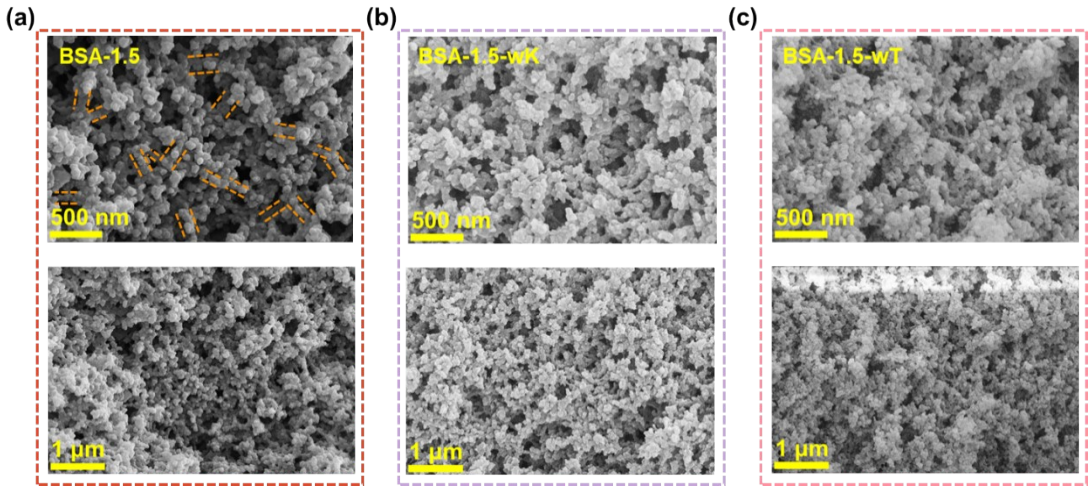

Fig. S13. SEM images of BSA-1.5 (a), BSA-1.5-wK (b), and BSA-1.5-wT (c).

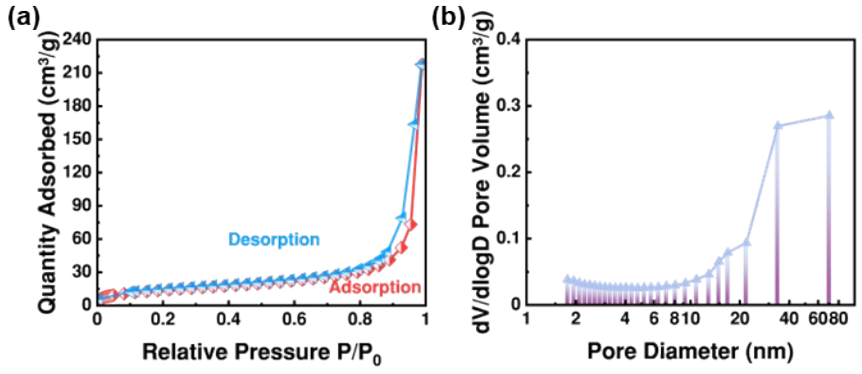

Fig. S14. Nitrogen isothermal adsorption curve (a) and BJH pore size distribution (b) of BSA-1.5-wK.

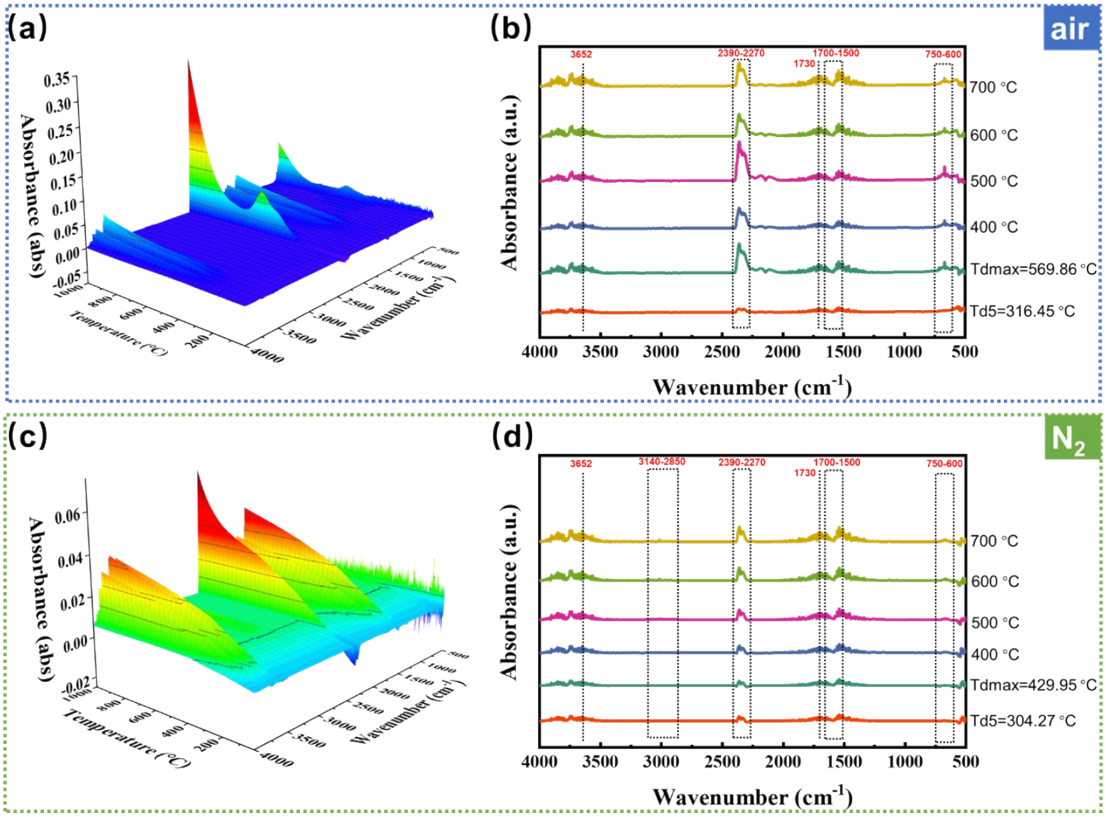

Fig. S15. TGA-FTIR testing of the BSA-1.5. (a) 3D color mapping surface plots in air atmosphere. (b) FTIR spectra at different temperatures under air atmosphere. (c) 3D color mapping surface plots in nitrogen atmosphere. (d) FTIR spectra at different temperatures under nitrogen atmosphere.

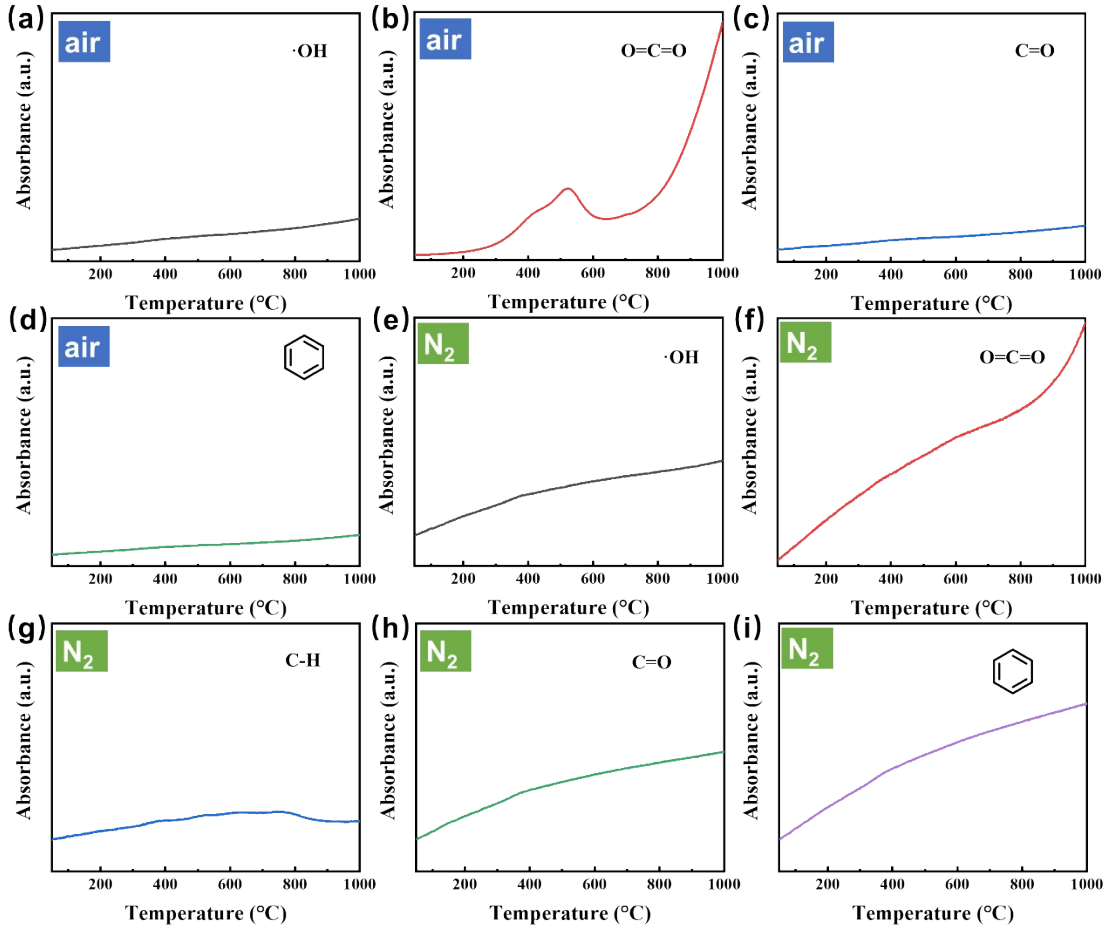

Fig. S16. Absorption intensity of several major FTIR peak signals at different temperatures. Under air atmosphere: (a) hydroxyl radical; (b) carbon dioxide; (c) formaldehyde; (d) benzene rings. Under nitrogen atmosphere: (e) hydroxyl radical; (f) carbon dioxide; (g) hydrocarbons; (h) formaldehyde; (i) benzene rings.

The volatiles during thermal degradation of BSA-1.5 in different atmospheres were tracked in real time using TGA-FTIR coupling. In air atmosphere, the released gaseous products mainly included -OH (3652 cm^{-1}), carbon dioxide (2390~2270 cm^{-1}), formaldehyde (1730 cm^{-1}) benzene ring/aromatic compounds (1700~1500 cm^{-1}, 750~600 cm^{-1}), and hydrocarbons (3140~2850 cm^{-1}) were added to this in the argon environment[1–4]. In an air atmosphere, the peak signals are most pronounced for carbon dioxide. Under argon, the peak signals are most pronounced for carbon dioxide and benzene ring/aromatic compounds.

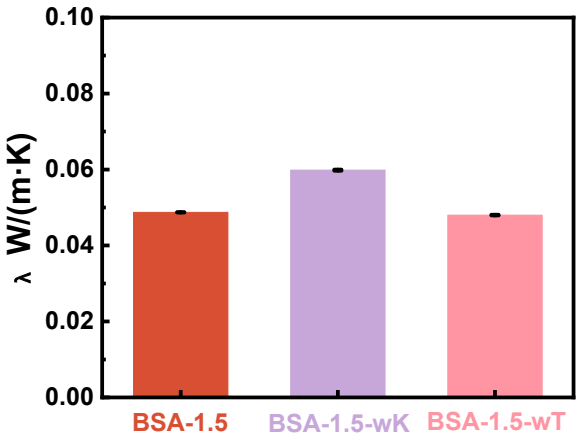

Fig. S17. Thermal conductivity of BSA-1.5, BSA-1.5-wK, and BSA-1.5-wT.

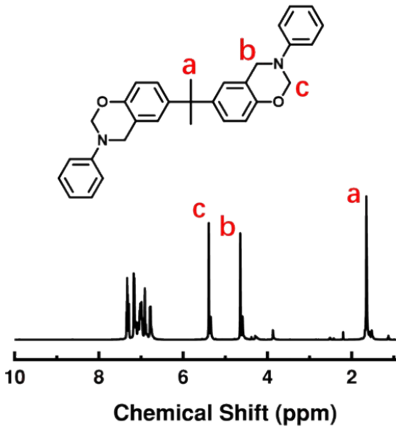

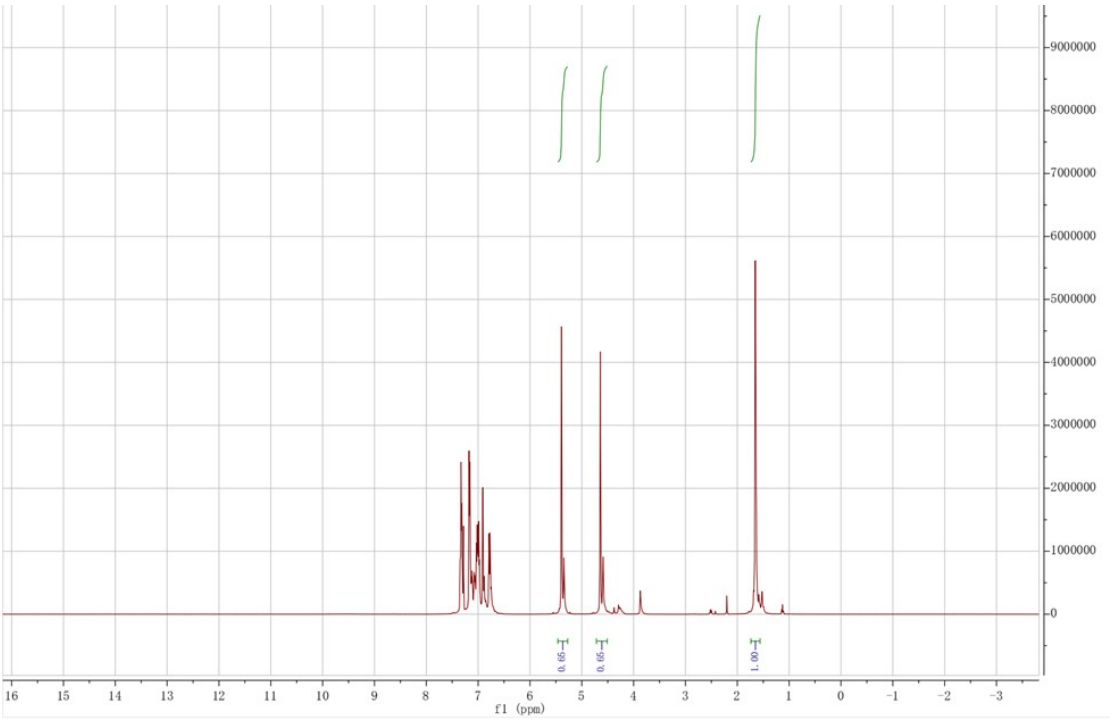

Fig. S18. ^{1}H NMR spectra of BzM.

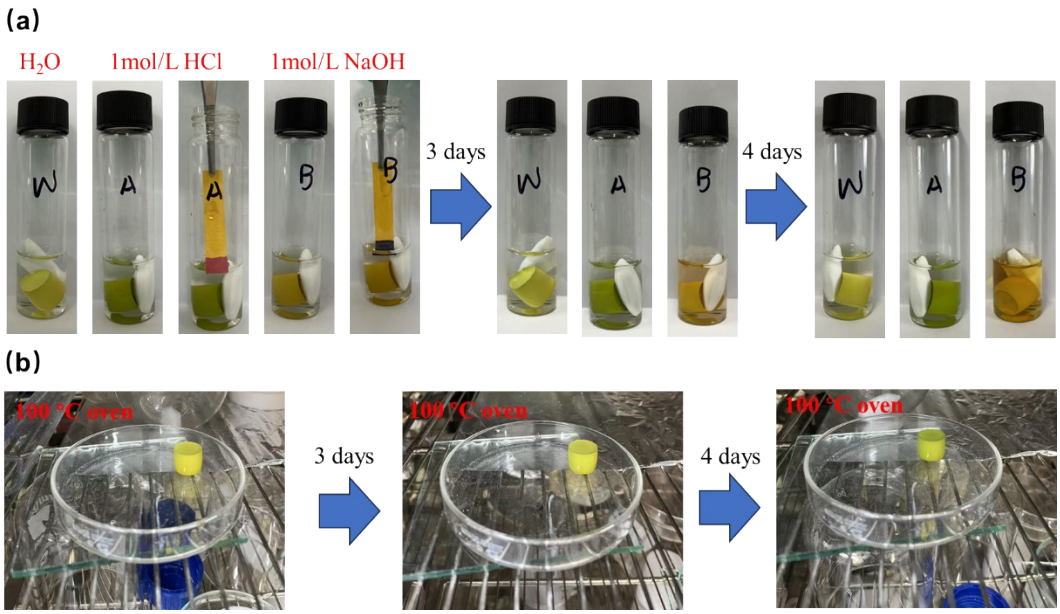

Fig. S19. Stability of BSA under high temperature, high humidity, strong acid, strong bases

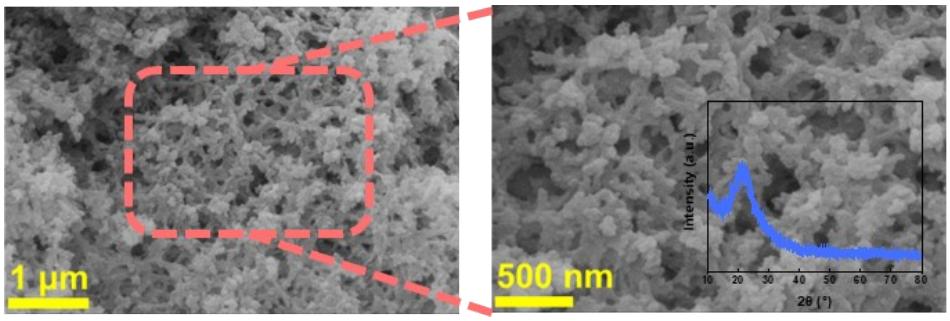

Fig. S20. Microstructure of amorphous silica fragments after pyrolysis in air atmosphere

Table S1. Individual ingredient dosage formulations for BSAs gel reaction

Sample	BzM (g)	hydrochloric acid (mL)	H_2O (mL)	TA (g)	MTMS (g)	KH-792 (g)	DMF (g)
BSA-0.6	7.20	1.00	1.75	0.50	3.75	0.25	12.25
BSA-1.0	6.00	1.00	1.75	0.50	5.75	0.25	12.25
BSA-1.5	4.80	1.00	1.75	0.50	6.95	0.25	12.25
BSA-2.0	4.00	1.00	1.75	0.50	7.75	0.25	12.25
BSA-1.5-wT	4.80	1.00	1.75	/	6.95	0.25	12.25
BSA-1.5-wK	4.80	1.00	1.75	0.50	6.95	/	12.25

Table S2. Heat resistance data of BSAs

Sample	Td5 (N_2, °C)	residual mass (N_2, %)	Peak temperature of heat loss (°C)	Td5 (air, °C)	residual mass (air, %)	Peak temperature of heat loss (°C)
BSA-0.6	291.25	23.58%	450.25	389.50	10.48%	609.50
BSA-1.0	309.25	49.43%	446.75	395.50	16.98%	586.50
BSA-1.5	312.75	60.09%	445.50	389.75	31.48%	594.75
BSA-2.0	348.25	69.31%	461.50	383.25	35.86%	596.50

Table S3. Flame retardancy data for BSAs

Sample	heat release rate (HRR, W/g)	heat release capacity (HRC, J/g·K)	total heat release (THR, kJ/g)
BSA-0.6	58.3	58.1	8.8
BSA-1.0	51.1	51.0	7.7
BSA-1.5	36.3	36.2	5.4
BSA-2.0	26.1	26.0	3.9

Table S4. Other performance data for BSAs

Sample	Thermal conductivity (W/m·K)	Water contact angle (°)	Average reflectance in the spectral region (%)
BSA-0.6	0.0684	70.54	76.93
BSA-1.0	0.0567	103.24	76.19
BSA-1.5	0.0487	122.04	79.27
BSA-2.0	0.0502	136.83	75.65

Table S5. Comprehensive performance comparison of BSA-1.5 and other PBz hybridized aerogels.

Sample	Thermal conductivity (W/m·K)	Compressive strength (MPa)	Td5 (in N_2 °C)	Td5 (in air °C)	Gelation temperature (°C)	HRR (W/g)	Ref.
BSA-1.5 (this work)	**0.0487**	**20.00**	**312.75**	**389.75**	**20**	**36.3**	
CBAs-T2	0.035	0.9	/	230	75	100	[5]
PBO/SiO2-1	0.035	6	180	/	20	82.1	[6]
PVMDMS-PBO -1	0.0467	3.4	90	/	20	104.2	[7]

PBz-30	0.0463	10.59	220	/	75	36.5	[8]
PSAs	0.064	7.74	/	220	60	/	[9]

Table S6. Comprehensive performance comparison of BSA-1.5 and other phenolic hybridized aerogels.

Sample	Thermal conductivity (W/m·K)	Compressive strength (MPa)	Td5 (in N_2 °C)	Td5 (in air °C)	Gelation temperature (°C)	Add fiber or not	Ref.
BSA-1.5 (this work)	**0.0487**	**20.00**	**312.75**	**389.75**	**20**	**no**	
NGF/PRA W-25	0.062	7.2	310	/	180	yes	[10]
TiCF/PR	0.312	2.1	/	355.3	180	yes	[11]
30	0.043	3	/	343.91	180	no	[1]
SiR/BPR-PR							
QCF/SPA-2	0.328	4.71	/	352	180	yes	[12]
CF/Si2/PR	0.093	0.98	312.98	344.07	180	yes	[13]
FCF/15RF	0.113	8.44	/	/	90	yes	[14]
SZR4	0.102	/	280	/	100	yes	[15]
C-QF/PSi100	0.183	9	297.64	/	180	yes	[16]
CBCF-PR/Si0.08	0.24	4	204.15	/	180	yes	[17]
γ-SP-RT-bd-3	0.063	2.5	378	/	60	no	[18]

Table S7. Average density of BSAs

Sample	Average density (g/cm^3)
BSA-0.6	0.417
BSA-1.0	0.376
BSA-1.5	0.320
BSA-2.0	0.146

References

1 T. Liu, W. Jiang, H. Qian, X. Shi, J. Chen, Q. Cao, N. Li, Y. Huang and B. Jiang, *Chemical Engineering Journal*, 2024, **482**, 149061.

2 K. Xue, Q. Wu, P. Zhang, Z. Song, H. Liu, M. Chai, X. Guo, S. Li and L. Liu, *Polymer Degradation and Stability*, 2024, **227**, 110856.

3 X. Shi, K. Zhang, J. Chen, H. Qian, Y. Huang and B. Jiang, *Adv Funct Materials*, 2024, **34**, 2311567.

4 K. Xue, P. Zhang, Z. Song, F. Guo, Z. Hua, T. You, S. Li, C. Cui and L. Liu, *Polymer Degradation and Stability*, 2025, **231**, 111092.

5 S. Zhang, Z. Wang, Y. Hu, H. Ji, Y. Xiao, J. Wang, G. Xu and F. Ding, *Biomacromolecules*, 2022, **23**, 5056–5064.

6 Y. Xiao, L. Li, H. Cai, F. Liu, S. Zhang, J. Feng, Y. Jiang and J. Feng, *J Appl Polym Sci*, 2021, **138**, 50333.

7 L. Li, Y. Xiao, S. Zhang, J. Feng, Y. Jiang and J. Feng, *J Sol-Gel Sci Technol*, 2023, **106**, 422–431.

8 S. Liu, Y. Xiao, J. Zhou, S. Zhang, L. Li, Z. Li and S. Xiong, *European Polymer Journal*, 2023, **196**, 112281.

9 S. Zhang, H. Ji, Z. Wang, Y. Xiao, Z. Yang, J. Wang, K. Lu, G. Xu, S. Xiong, Z. Li, Y. Yang and F. Ding, *ACS Appl. Polym. Mater.*, 2022, **4**, 6602–6611.

10 C. Wu, L. Wang, X. Yan, H. Huang, Y. Pan, H. Wang, W. Wang, S. Yuan, J. Fan, X. Jin, C. Hong and X. Zhang, *Composites Science and Technology*, 2024, **256**, 110776.

11 Y. Pan, X. Jin, H. Wang, H. Huang, C. Wu, X. Yan, C. Hong and X. Zhang, *Journal of Materials Science & Technology*, 2023, **152**, 181–189.

12 X. Jin, C. Wu, H. Wang, Y. Pan, H. Huang, W. Wang, J. Fan, X. Yan, C. Hong and X. Zhang, *Composites Science and Technology*, 2023, **232**, 109878.

13 C. Wang, H. Cheng, C. Hong, X. Zhang and T. Zeng, *Composites Part A: Applied Science and Manufacturing*, 2018, **112**, 81–90.

14 X. Liu, J. Sun, F. Yuan, C. Ye and R. Zhang, *J of Applied Polymer Sci*, 2022, **139**, 51712.

15 H. Fu, Y. Qin, Z. Peng, J. Dou and Z. Huang, *Ceramics International*, 2024, **50**, 21008–21019.

16 H. Cheng, Z. Fan, C. Hong and X. Zhang, *Composites Part A: Applied Science and Manufacturing*, 2021, **143**, 106313.

17 R. Yin, H. Cheng, C. Hong and X. Zhang, *Composites Part A: Applied Science and Manufacturing*, 2017, **101**, 500–510.

18 Y. Xue, X. Meng, B. Yuan and H. Xu, *Materials Chemistry and Physics*, 2023, **305**, 128024.